Journal of the Korean Society of Oceanography
Vol. 34, No. 1, pp. 1—21, March 1999

Self-excited Variability of the East Korea Warm Current: A Quasi-Geostrophic Model Study

SANG-KI LEE
Department of Oceanography, Inha University, Incheon 402-751, Korea

A two-layer quasi-geostrophic numerical model is used to investigate the temporal variability of the East Korea Warm Current (EKWC), especially the separation from the Korean coast and the generation of warm eddies. An attention is given on the active role of the nonlinear boundary layer process. For this, an idealized flat bottom model of the East Sea is forced with the annual mean wind curl and with the inflow-outflow specified at the Korea (Tsushima) and Tsugaru Straits. Two types of separation mechanisms are identified. The first one is influenced by the westward movement of the recirculating leg of the EKWC (externally driven separation), the second one is solely driven by the boundary layer dynamics (internally driven separation). However, these two processes are not independent, and usually coexist. It is hypothesized that "internally driven separation" arises as the result of relative vorticity production at the wall, its subsequent advection via the EKWC, and its accumulation up to a critical level characterized by the separation of the boundary flow from the coast. It is found that the sharp southeastern corner of the Korean peninsula provides a favorable condition for the accumulation of relative vorticity. The separation of the EKWC usually accompanies the generation of a warm eddy with a diameter of about 120 km. The warm eddy has a typical layer-averaged velocity of 0.3 m/s and its lifespan is up to a year. In general, the characteristics of the simulated warm eddy are compatible with observations. A conclusion is therefore drawn that the variability of the EKWC is at least partially self-excited, not being influenced by any sources of perturbation in the forcing field, and that the likely source of the variability is the barotropic instability although the extent of contribution from the baroclinic instability remains unknown. The effects of the seasonal wind curl and inflow-outflow strength are also investigated.

INTRODUCTION

The East Korea Warm Current (EKWC hereafter) is a western boundary current flowing northward along the east coast of Korean peninsula, frequently observed to turn offshore at 36°N~38°N (Yi, 1966; Seung, 1992a). As the EKWC separates from the coast, a recirculation gyre is usually developed, in effect a warm eddy is often formed near the southwest of Ullung Island (Moriyasu, 1972). When this happens, the EKWC assumes the form of a meandering flow, thereby spawning a number of sporadic eddies with diameters of some 100 km. This characteristic of the EKWC is typical of western boundary currents, such as the Gulf Stream along the east coast of U.S. Similarly to other western boundary currents, the EKWC plays significant roles in the basin-wide circulation and the heat budget (Seung, 1992a; Lie and Seung, 1994). It is, therefore, vital to understand the physics underlying the variability of EKWC, to better describe the circulation dynamics in the East Sea (Japan Sea).

Historically, the EKWC has been considered to be a permanent feature (Suda and Hidaka, 1932; Uda, 1934; Kawabe, 1982). However, Kim and Legeckis (1986) showed, based on the analysis of AVHRR SST images, that the connection between the EKWC and the Tsushima Current (TC hereafter) is highly variable in nature, therefore the EKWC can be absent depending on observation period, contrary to the branching hypotheses originally proposed by Uda (1934). In fact, there are a number of observational studies which show significant temporal variations of the EKWC (e.g., An and Chung, 1982; Gong and Son, 1982; Hong and Cho, 1983).

At this stage, however, it is far from clear exactly what causes the temporal variation of the EKWC.

Since the EKWC originates directly from the TC, it is usually postulated that the variation of the TC is an important source of the variability. This line of possibility was explored by An and Chung (1982): analyzing the fluctuations of the polar front which roughly coincide with the axis of the EKWC, they suggested that the north-south directed fronts (EKWC) may be strengthened by the supply of warm water from the TC. More recently, Isoda and Saito (1993) studied a similar problem, and showed that temporal variability of the EKWC can be initiated by the perturbation of the TC. Based on a series of infra-red SST images and hydrographic data, they further suggested that the perturbation may eventually grows into an isolated eddy with a horizontal size of some 100 km in diameter.

Other conceivable causes of the EKWC variability include the seasonally varying wind, wintertime cooling (subduction and convection) in the northern East Sea, and hydrodynamic instabilities. The influence of the seasonal wind was investigated numerically by Seung (1992b) and Kim and Yoon (1996) which are discussed in the later section. The role of wintertime cooling is most perplexing since the convection (or subduction) takes place strictly in the northern East Sea, therefore it works as a remote forcing. Nevertheless, there are a couple of interesting studies which attempted to associate the convection (or subduction) with the seasonal variation of the EKWC (Kim and Legeckis, 1986; Seung and Nam, 1992; Seung and Kim, 1995). Particularly, Kim and Legeckis (1986) suggested that the cold water mass subducted from the mixed layer in the northern East Sea strengthens the polar front which in turn prevents the EKWC from extending northward.

Western boundary currents has long been known to be susceptible to instabilities, and the EKWC is certainly not an exception. Unfortunately, however, the potential roles of hydrodynamic instabiliies on the EKWC have never been explored, whereas it is a critical element comprehending the physics of western boundary currents (Csanady, 1989; Ierley and Young, 1991). Therefore, it is the objective of this study to identify and to understand the physical principles underlying the temporal variability of the EKWC focusing on instabilities and nonlinear boundary layer processes of the EKWC, with a help of a two-layer quasi-geostrophic (QG) model. Undoubtedly, there are many restrictions in the QG approximation. However, it still best fits the interest of this study. In the following chapters, previous modeling studies are briefly reviewed and the model formulation is described, followed by the presentation of model results and discussion. The impacts of seasonal wind curl and TC strength are investigated afterward.

PREVIOUS MODELING STUDIES

To comprehend the complex dynamics of the EKWC, a few numerical model studies have been attempted. In particular, these studies have focused on the mechanism of the EKWC separation. Among those, Seung (1992b) used a linear quasi-geostrophic (QG) model to show that the separation of the EKWC is determined by the relative strength of the inflow-outflow and the surface vorticity flux such as the surface cooling and the wind stress curl. Kim and Yoon (1996) further tested this hypotheses using a nonlinear 1 ½ layer model, but the results were nearly identical to those reported by Seung (1992b).

There is a series of primitive equation model studies (e.g., Yoon, 1982; Kim, 1991; Seung and Kim, 1993; Kim, 1996). However, the simulated EKWC by these complex numerical models are, in many respects, unrealstic. Especially, the overshooting of the EKWC was a common problem in these model studies. Among others, Seung and Kim (1997) applied an isopycnal coordinate model to the East Sea, and obtained a more realistic result in the separation latitude of the EKWC, although it is skeptical if the horizontal resolutionrm (0.5°) of their model was fine enough to resolve the western boundary layer.

Recently, a QG model was used by Lim and Kim (1995) to study the effect of bottom topography on the pathway of the TC. They specified the spatial distribution of the TC with a sinusoidal signal of one year period, maintaining a constant 3.0Sv (see Fig. 4 in Lim and Kim, 1995). Their model result showed that the realistic meandering of the TC is possible only with this signal. It appears that their choice of slip boundary condition along the western boundary, by which the role of boundary layer process diminished considerably, was responsible for this result. Another point is that there appears to be an inadequacy in their idealized topography: distinctive topography features such as Ullung basin or Yamato rise were all removed and only coastal slope was included, by which the model certainly

violated the QG assumption (Pedlosky, 1979; Holland, 1986).

MODEL FORMULATION

Governing equations

Consider an ocean consisting of N active layers of different densities. Then, following Pedlosky (1979), the layer-averaged vorticity equation on a β-plane is

$$\frac{\partial}{\partial t}\nabla^2\psi_k = J(\nabla^2\psi_k,\ \psi_k) - \beta\frac{\partial\psi_k}{\partial x} + \frac{f_o}{H_k}(w_{k-\frac{1}{2}} - w_{k+\frac{1}{2}}) + A_h\nabla^4\psi_k - \delta_{N,k}\varepsilon\nabla^2\psi_n + \delta_{1,k}\frac{\mathrm{curl}_z\,\tau}{\rho_1 H_1}, \qquad \text{for k=1, 2, ..., N,} \tag{1}$$

where ψ_k is the streamfunction of each layers, H_k is the mean layer thickness, $w_{k+\frac{1}{2}}$ is the vertical velocity at the layer interface, $J(a,\ b)$ is the Jacobian operator, A_h is the lateral eddy viscosity, ε is the linear bottom friction coefficient, δ_{ij} is the Kronecker delta, and $f(=f_o+\beta y)$ is Coriolis parameter. The continuity equation is

$$\frac{\partial\eta_{k+\frac{1}{2}}}{\partial t} = J(\eta_{k+\frac{1}{2}},\ \psi_{k+\frac{1}{2}}) + w_{k+\frac{1}{2}}, \quad \text{for k=1, 2, } \cdots\text{, N-1,} \tag{2}$$

where the interfacial displacement and the streamfunction have following relationship

$$\eta_{k+\frac{1}{2}} = -\frac{f_o}{g'_{k+\frac{1}{2}}}(\psi_k - \psi_{k+1}), \text{ for k=1, 2, } \cdots\text{, N-1,} \tag{3}$$

where $g'_{k+\frac{1}{2}}$ is the reduced gravity given by

$$g'_{k+\frac{1}{2}} = \frac{g(\rho_{k+1}-\rho_k)}{\rho_o}, \quad \text{for k=1, 2, } \cdots\text{, N-1.} \tag{4}$$

Bottom topography is incorporated in the model through the bottom boundary condition on the vertical velocity:

$$w_{N+\frac{1}{2}} = -J(h_B,\ \psi_N). \tag{5}$$

The interface streamfunctions are calculated as weighted average of the layer streamfunctions (Holland, 1978):

$$\psi_{k+\frac{1}{2}} = \frac{H_{k+1}\psi_k + H_k\psi_{k+1}}{H_k + H_{k+1}}, \quad \text{for k=1, 2, } \cdots\text{, N-1.} \tag{6}$$

An additional constraint is the mass conservation in each layer (McWilliams, 1977):

$$\iint_\Omega w_{k+\frac{1}{2}}\,dxdy = 0, \quad \text{for k=1, 2, } \cdots\text{, N-1,} \tag{7}$$

where the subscript Ω represents the integration over whole basin. The formulation of the multilayer quasi-geostrophic model is identical to that of the models described by Holland (1978) and Cummins and Mysak (1988).

Eqns. (1)~(7) are solved numerically in finite difference domain. The detail of the solution technique is described in the Appendix A.

Model geometry

The model covers the entire East Sea from 33.5°N to 45°N in longitudinal and from 127.5°E to 140°E in longitudinal directions, respectively, which is about 1280 km × 1080 km (see Fig. 1). To comply with the constraint of the QG approximation, the sidewall boundary of the Korean peninsula is

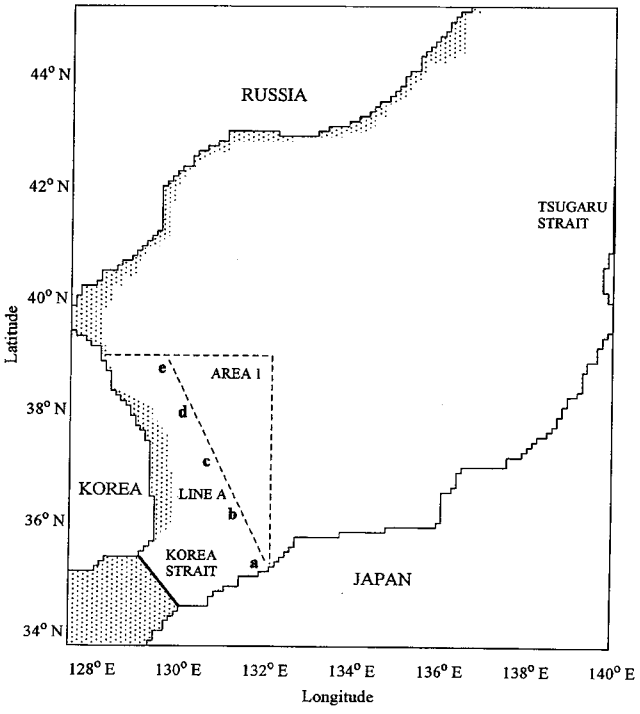

Fig. 1. The model configuration and the definition of area 1 and line A. The open boundaries are represented by thicker lines. The shaded area (H_T<200 m) is treated as a wall boundary.

chosen to coincide as nearly as possible with 200 m isobath line, while no such careful consideration is made for the sidewall boundary of the Japanese coast. The width of the two openings, Korea and Tsugaru straits are set equal to 127.3 km and 100 km, respectively.

Numerical formulation

The model equations are discretized in space on an Arakawa A grid scheme (Arakawa, 1966). The grid size is 10 km in both horizontal directions, therefore, the model domain contains 128×108 grid points per layer for each variables. The leapfrog time integration scheme is used with a time step of about 1/4 day. The forward time integration is applied every 40 time steps to remove the computational mode of the leapfrog scheme (Holland, 1978). The frictional terms are lagged one time step to avoid numerical instability (Richtmyer, 1967). To solve elliptical equations (A12, A15), the successive over relaxation (SOR) method is used (Roache, 1975).

Boundary conditions

In order to include frictional boundary effects, a no-slip condition is applied along the sidewall of the Korean peninsula. Along the west coast of Japan, on the other hand, the bottom controlled boundary current may not be properly represented in the QG model configuration since the QG approximation does not allow severe bottom slope. Therefore, for the sake of simplicity, the first branch of the TC is neglected in this study. Due to this reason, a free-slip condition is applied along the Japanese coast, which in turn removes the possible artificial boundary flow there. At the inflow boundary, relative vorticity is calculated subject to the prefixed shape of the TC, which is described in the next section, and the tangential velocity is set equal to zero. At the outflow boundary, a simple sine function is used to represent velocity distribution. Similarly to the conditions at the inflow boundary, relative vorticity is calculated subject to prefixed velocity distribution, and the tangential velocity is set equal to zero.

Verron and Blayo (1996) suggested that the accuracy in the numerical scheme for the no-slip boundary condition may influence the separation latitude. Therefore, a special attention is given to evaluate vorticity at the western boundary. Foreman and Bennett (1988), Verron and Blayo (1996) showed that the first order scheme is as accurate as the third order scheme if the model grid is fine enough to resolve the frictional boundary layer. Therefore, the first order scheme is used at the no-slip boundary. To estimate vorticity at oblique wall, the streamfunction at the nearest point perpendicular to the wall is used, which is the method No. 4 in Roach (1975). It was shown by Foreman and Bennet (1988) that this first order scheme gives results equivalent accuracy to higher order forms.

RESULTS

A preliminary experiment

To accurately simulate the East Sea circulation, the seasonally varying wind and TC, and variable bottom topography effects must be included. The impact of these factors on the EKWC will be considered later in the following sections, but first, here we investigate a simple case for which a flat-bottom, two-layer ocean is forced by the annual mean wind stress curl (Fig. 2). This model result will be used as the reference case. For this part of the model experiment, we set $H_1 = 200$ m, $H_2 = 1300$

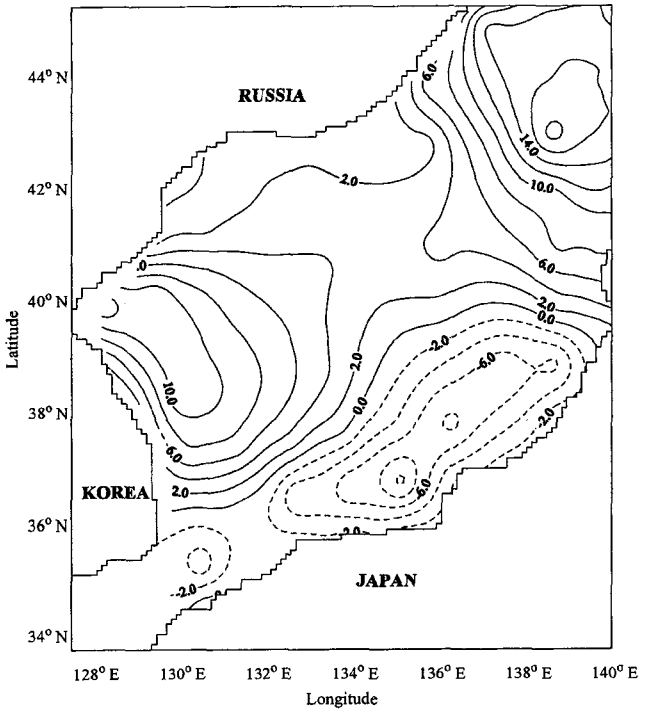

Fig. 2. Annual mean wind stress curl (Na *et al.*, 1992). The unit is 10^{-8}N/m^2.

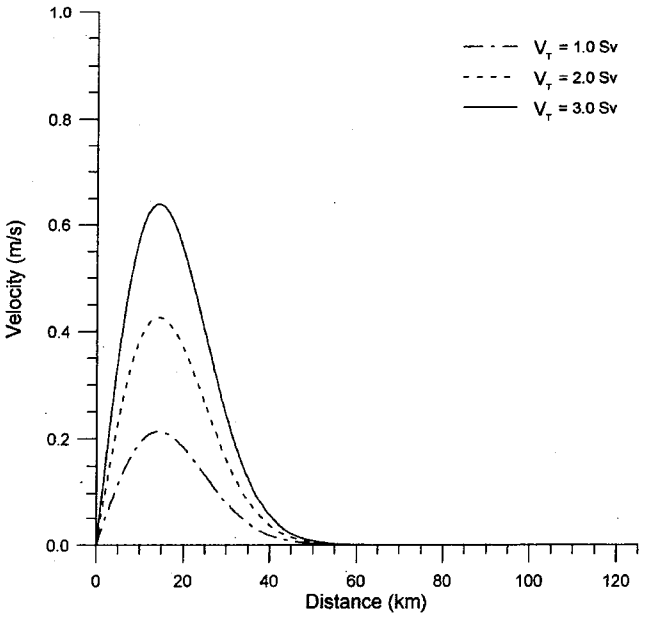

Fig. 3. The spatial profile of Tsushima Current when the total transports are 1.0, 2.0 and 3.0 Sv.

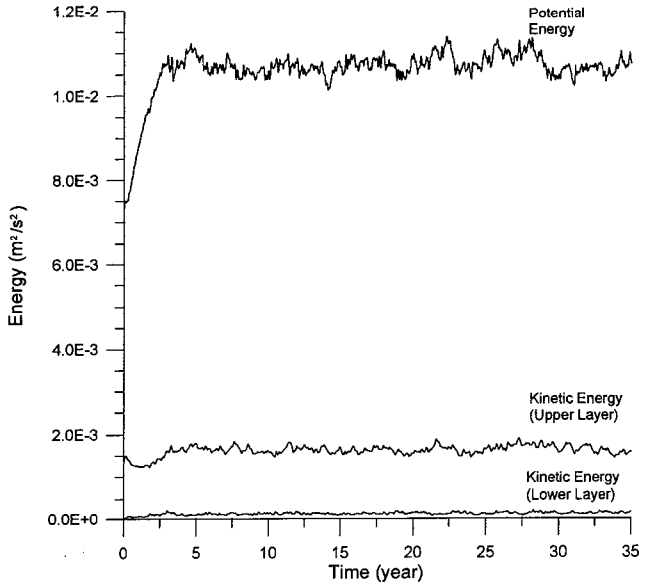

Fig. 4. The evolution of the kinetic energy of the two layers and the potential energy, all averaged over unit mass (in m^2/s^2).

m, $f_o=10^{-4}s^{-1}$, $\beta=2\times10^{-11}s^{-1}m^{-1}$, and $\varepsilon=10^{-7}s^{-1}$. The value of the lateral eddy diffusion coefficient is set to $100m^2s^{-1}$, which gives the Munk layer thickness $\delta_M=(A_h/\beta)^{1/3}$ of about 17km. Therefore, the model grid resolution of 10 km resolves the frictional boundary layer. The reduced gravity g' is set equal to $1.2\times10^{-2}m/s^2$ which yields the baroclinic deformation radius $R_1\simeq(\sqrt{g'H_1H_2/H})/f_o$ of 14.4 km. Since most unstable mesoscale eddies have a typical length scale of the baroclinic deformation radius (Charney, 1947; Eady, 1949), the model grid resolution is for eddy resolving. The TC is confined to the upper layer only, and its spatial profile is assumed as shown in Fig. 3 similar to that observed (Kaneko *et al.*, 1991) with the total volume flux (V_T) through the Korea Strait of 2.0Sv is chosen. The volume transport through the eastern channel is intentionally removed to preclude the ageostrophic boundary current along the Japanese coast, which is not well resolved by QG dynamics.

Fig. 4 shows the evolution of the kinetic energy of the two layers and the potential energy. It appears that the model attained a statistically steady state after 1800 days. Fig. 5 shows a sequence of the upper layer flow from 3600 days to 3930 days. The separation of the EKWC from the Korean coast and the subsequent generation of warm core eddies are clearly observed.

An interesting point is that the separation of the EKWC is usually triggered by the emerging cyclone at the sharp southeastern corner of the Korean peninsula (see Fig. 5(e)). Similar features to this were investigated previously by Dengg (1993) for the Gulf Stream: based on a series of barotropic numerical model experiments, Dengg suggested that the western boundary current may separate at sharp convex corner if required conditions are met. The requirements are that the boundary layer must exist (no-slip), and the Reynolds number of the flow exceed its critical value. Obviously, his statement is not new, but Prandtl (1935) presented a similar argument much earlier in his classical boundary layer separation theory.

Dengg (1993) also gave a physical explanation why the nonlinear evolution at the western boundary, especially at the sharp corner, may be an important factor which initiate the separation. For this, he used a rather complex path-integrated vorticity equation along the separated streamlines, but the physical idea was based on a hypotheses that the western boundary current separation arises as the result of relative vorticity production at the wall, its subsequent advection via the western boundary current, and its accumulation up to a critical level characterized by the separation of the boundary flow from the coast. If the western boundary current separation may take place due to this mechanism, a sharp convex corner provides a favorable condition for the accumulation of relative vorticity. In order to

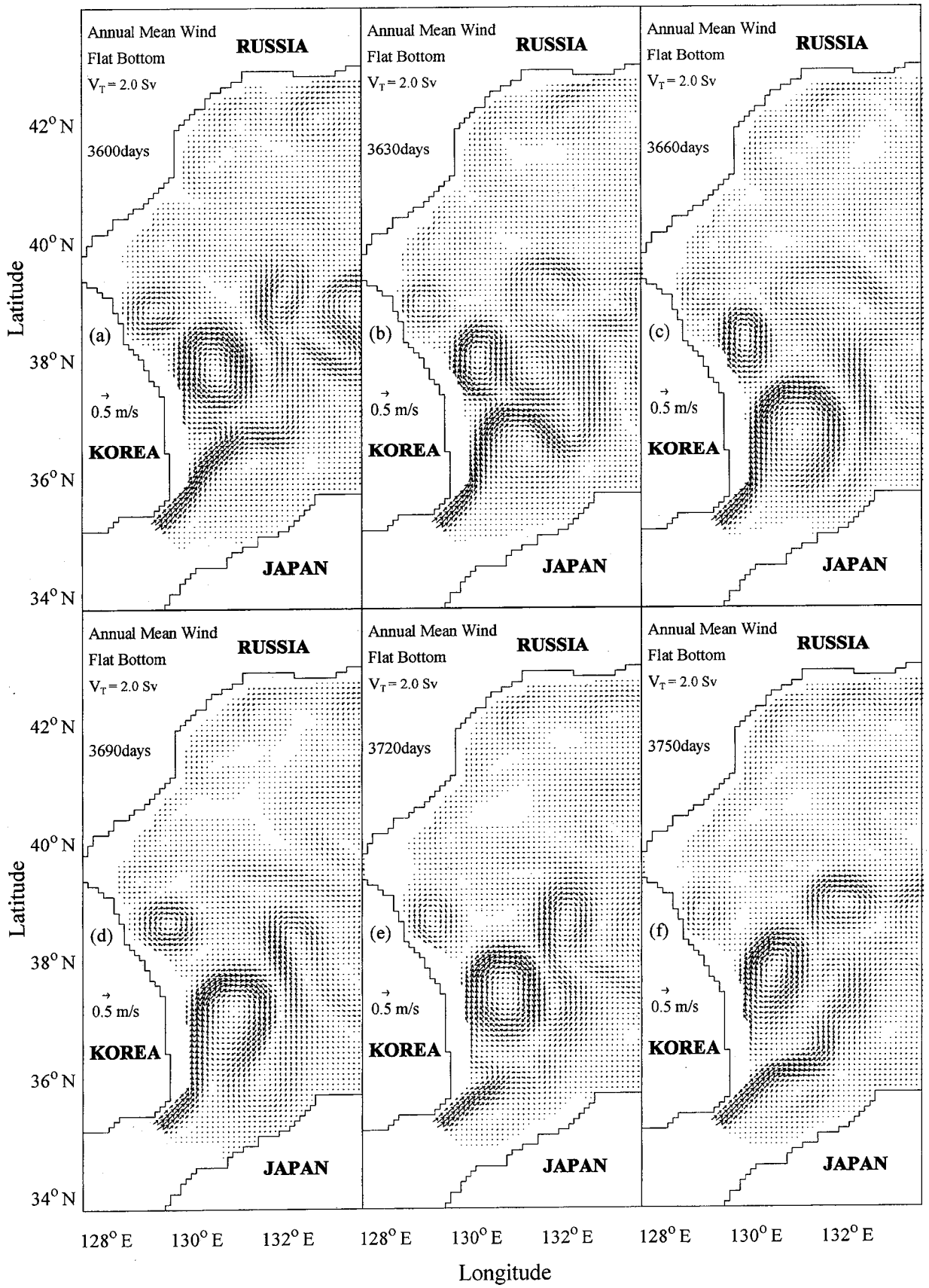

Fig. 5. A sequence of the upper layer flow from 3600 days to 3930 days for the preliminary experiment.

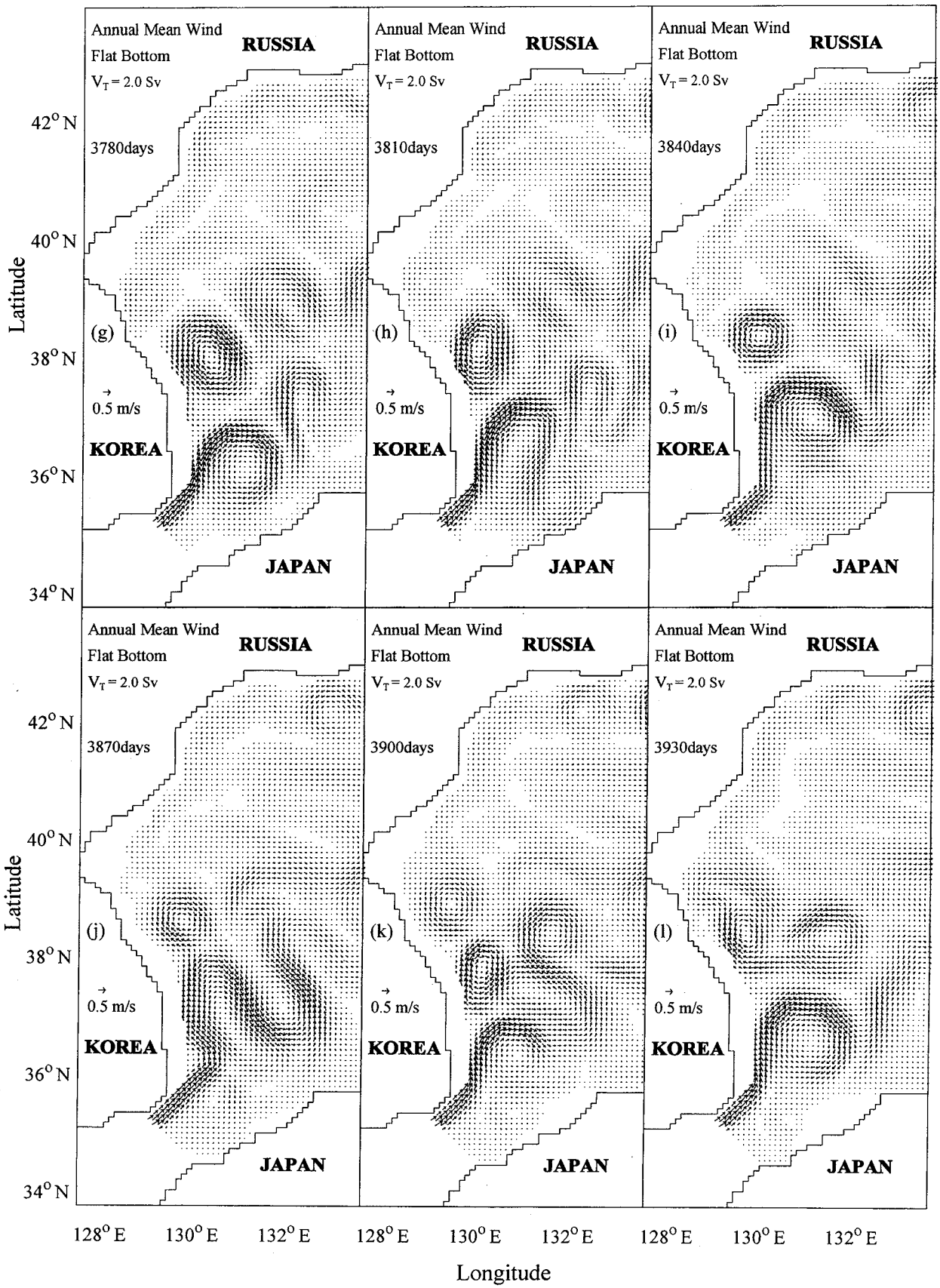

Fig. 5. Continued.

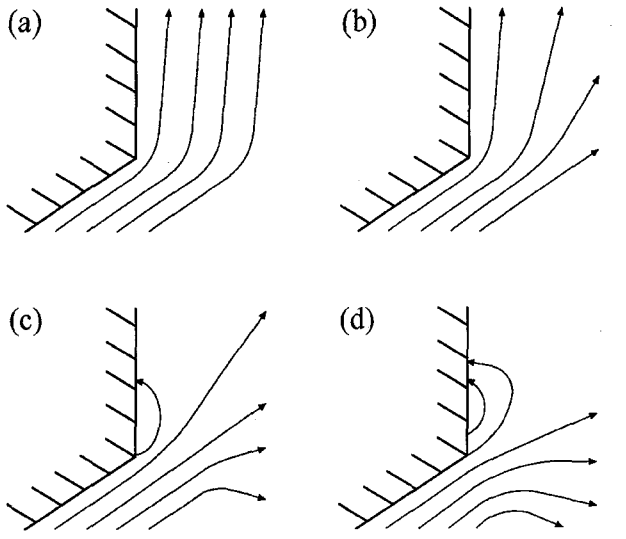

Fig. 6. A simple illustration showing the mechanism of boundary current separation at a sharp corner.

better describe this mechanism, a simple illustration is given in Fig. 6. If the flow has a low Reynolds number initially, the western boundary current is governed by the Munk regime (Munk, 1950). Therefore, the streamlines must be closely packed near the coast as shown in Fig. 6(a). If the Reynolds number increases gradually, the flow in the inertial boundary layer overshoots while the streamline inside the Munk layer is still intact along the coastline (Fig. 6(b)). Still, this does not explain why the western boundary current separates from the coast. As the overshooting continues, the streamlines in the downstream of the corner become broader, then relative vorticity near the coast is forced to accumulate at the sharp convex corner. After the accumulation reaches a critical value, the western boundary current must separate from the coast (Fig. 6(c)). In turn, to conserve potential vorticity, the separated boundary current gains a negative vorticity (positive vorticity for the southward boundary current), then recirculates southward (Fig. 6(d)) (Cessi et al., 1987). It appears that the flow structures in Fig. 5(i)~5(k) show the separation of the EKWC at the sharp corner due to the mechanism just described.

However, it must be pointed out that, obviously there are other influences. If the separation mechanism described above is denoted as "internally driven separation", "externally driven separation" is also observed in Fig. 5(d)~5(f); it is clear that the recirculation gyre is formed, and its leg is moving toward the Korean coast possibly (but not certainly) as a form of the Rossby wave. A similar result was previously reported from the hydrographic data analysis carried out by An *et al.* (1994). By comparing the movement speed of the observed eddies with the phase speed of the internal Rossby wave, they suggested that the movement of warm eddies or the recirculation leg in this case may be influenced by the Rossby wave. Whatever the reason, as the recirculation leg approaches the Korean coast, the boundary current changes its direction toward south, which induces the accumulation of relative vorticity at the point where the recirculation leg collides with the coast. In this case, the sharp corner is not a necessary condition for the separation, but the flow may separate at any place to the downstream of the convex corner. Therefore, unlike the internally driven separation case, the externally driven separation does not always accompany the cyclonic eddy at the sharp corner. It must be pointed out, however, that these two different separation processes are not independent, and usually coexist.

It is noticed from Fig. 5 that the EKWC continually generates warm core eddies with a diameter of about 120 km and with a typical layer-averaged velocity of 0.3 m/see. The warm eddies then move slowly toward north, during which its size and strength are diminished until it eventually die out. This model feature is compatible with the sequence of AVHRR images taken from Fisheries Research and Development Agency, Korea shown in Fig. 7(a)~7(c). The generation of a warm core ring followed by the northward advection are fairly well observed.

Further evaluation of the model result shows that approximately two eddies are formed in one year period. This can be readily observed in Fig. 8 which shows a time-distance plot of the upper layer streamfunction along the line A (see Fig. 1 for definition). The thicker line roughly coincides with the northern edge of the separated EKWC. According to this, the northern edge moves about 250 km in 150 days period, which yields the speed of about 0.02 m/s. This may roughly represent the northward moving speed of warm eddies. Apart from this, the figure clearly shows that the detachment of warm eddies takes place abruptly with the period of approximately 6 months. It is also noticed that the lifespan of one eddy lasts up to one year.

Although there are not enough observational evidence to fully validate the model result, Shin

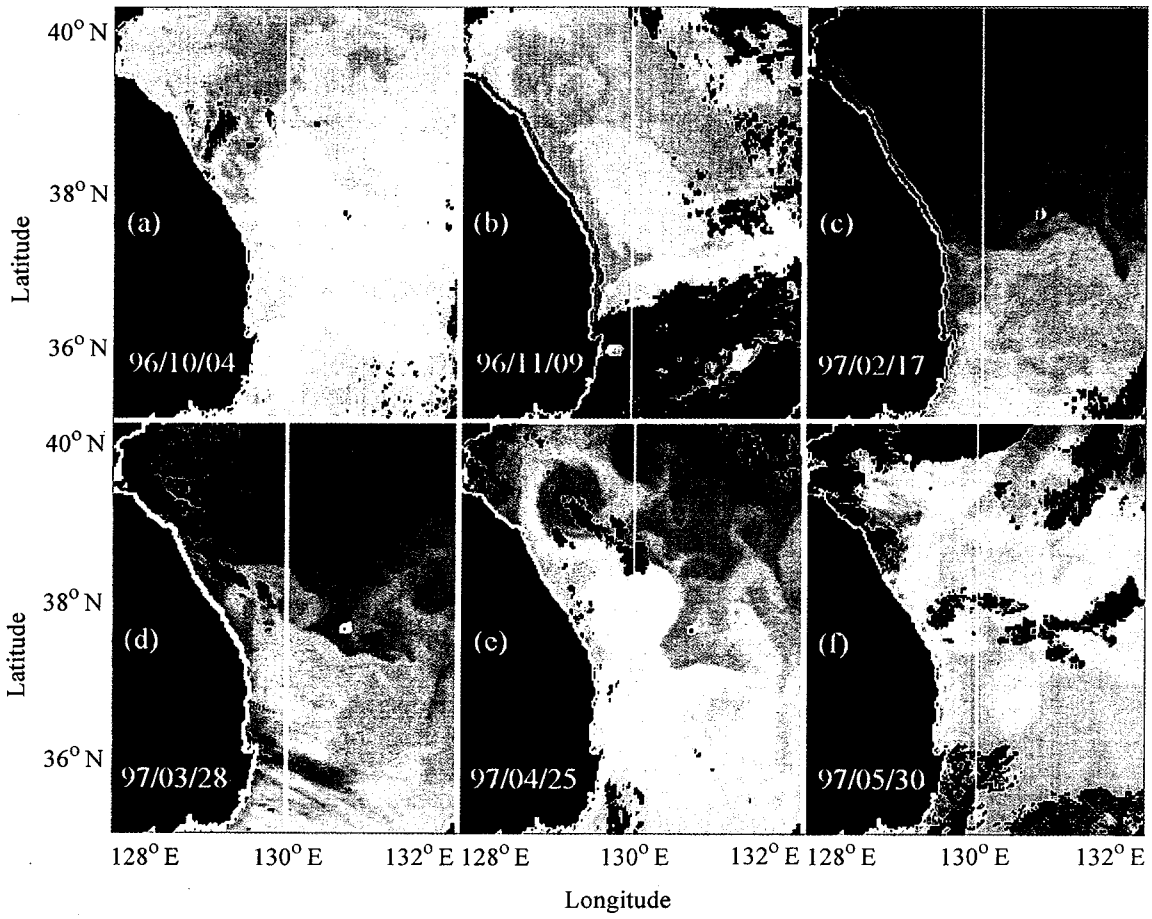

Fig. 7. A sequence of AVHRR SST images taken from Fisheries Research and Development Agency, Korea. Darker (brighter) tones represent warmer (colder) area in general.

et al. (1995) gives a clue that the characteristics of the modeled warm eddy are reminiscent of those observed. Based on hydrographic data and AVHRR images, they studied the behavior of a warm eddy, observed for about 6 months from October 1991 to June 1992, with the size of roughly 130~160 km in diameter. The warm eddy was formed before October 1991, and the diameter was about 160 km in March 1992. Its size decreased to 140 km in June 1992 and the core moved slightly northward. Then it moved east and northward until it disappeared in October 1992. The lifespan, the speed of movement and the size of the warm eddy are all compatible with the features of the simulated warm eddy. Furthermore, Shin *et al.* (1995) found that the eddy is in nearly geostrophic balance with a maximum velocity of 0.65 m/s at the sea surface. If the geostrophic velocity is assumed to decrease linearly down to zero at the base of the eddy, the layer averaged velocity is about 0.33 m/s, which also agrees well with the model result.

There are a couple of other observational studies on the characteristics of the warm eddy, which also supports our model result. Based on the hydrographic data gathered by Fisheries Research and Development Agency, Korea from 1967 to 1986, An *et al.* (1994) found that the warm eddies are 130km in diameter, and move west, north and southward with a mean speed of 0.8~2.5 cm/s, or stay over a few months at the same place southwestward of the Ullung Island. Our model results show the warm eddy with a size of 120 km in diameter, with a typical movement speed of 2.0 cm/s, which agrees well with their observations.

Effect of Tsushima Current strength

It is well established from observations that the volume flux through the Korea Strait changes seasonally as well as interannually (Hidaka and Suzuki, 1950; Yi, 1966; Toba *et al.*, 1982; Egawa *et al.*, 1993; Isobe *et al.*, 1993; Kawano, 1993; Isobe,

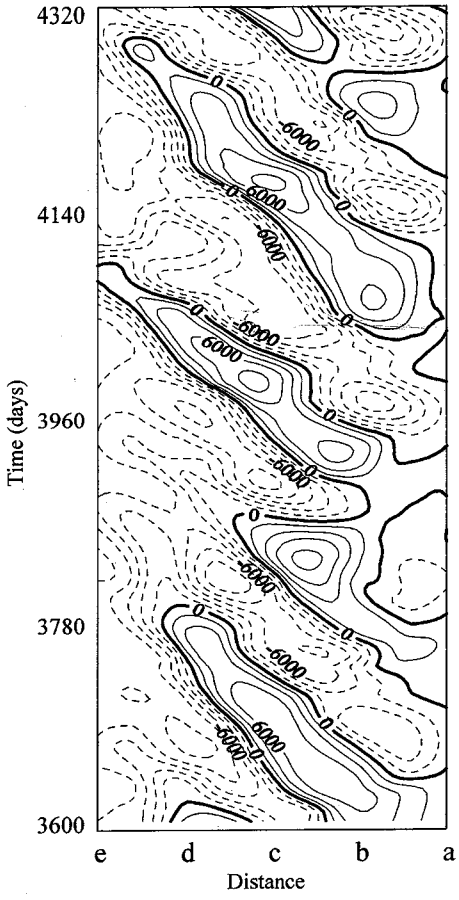

Fig. 8. A time-distance plot of the upper layer stream function along the line A for the preliminary experiment.

1994). Therefore, here we explore how the different values of the volume flux through the Korea Strait change the temporal and spatial structures of the EKWC. We carry out two model experiments with the identical parameter values to the reference case, except that the volume fluxes (V_T) are set equal to 1.0 and 3.0Sv. Before we go further, to check whether the two cases are potentially unstable, here we examine the instability analysis of western boundary currents, carried out by Ierley and Young (1991). Solving the Orr-Sommerfeld equation which was modified to include beta-effect, they studied the barotropic instability of frictional western boundary currents, i.e., the Munk regime. They found that the critical Reynolds number, at which the flow become unstable, is in between 20 and 100 depending on the mean flow profiles. Applying this to our case, if we take the Munk Layer thickness as the boundary layer length scale, it is found that the critical TC velocity at which the barotropic instability to occur may be as low as 0.1 m/s. Obviously, there are many overidealized aspects in their model. For instance, the western boundary current was assumed to be parallel to the wall, and the baroclinic instability was not considered. Nevertheless, the application of their result suggest that the two cases considered here are potentially unstable to small perturbations, since the velocity scale of the TC is 0.2 m/s and 0.64 m/s when $V_T=1.0$Sv and $V_T=3.0$Sv, respectively (see Fig. 3). Fig. 9 and Fig. 10 show sequences of the upper layer velocity for $V_T=1.0$Sv and $V_T=3.0$Sv cases, respectively. It appears that the separation is mainly "externally driven" when $V_T=1.0$Sv, while "internally driven separation" continues to occur when the volume flux is increased to 3.0Sv.

Other than that, when $V_T=1.0$Sv, the northern limit of the EKWC excursion moves much northward at about 39°N and no significant time change is detected in its position, the flow is much more organized, and the eddy generation rate is slower (only one eddy is detected in one year period). The AVHRR images shown in Fig. 7(d)~7(f) is taken in the spring of 1997 when the TC transport is believed to be minimum. These images appears to be similar to the model result shown in Fig. 9. On the other hand, when the volume flux is increased to 3.0Sv, the separation usually takes place at the convex corner, the northern limit of the EKWC excursion moves between 35°N and 38°N, the eddy generation rate is much faster (about 3 eddies are detected in one year period), and the flow is less organized hardly repeating same spatial pattern in time.

It appears that these model results are due to that the stronger TC tends to accelerate the boundary flow, so that the vorticity accumulation at the corner takes place much faster and stronger, and vice versa. Therefore, it can be concluded that, for the low Reynolds number flow, "externally driven separation" dominates, while "internally driven separation" plays a significant role for the high Reynolds number flow.

Role of wind stress curl

To further understand the role of the wind stress curl on the separation of the EKWC and eddy generation, we carry out an experiment in which the wind is turned off and the model is driven only by the inflow (TC). The result is shown in Fig. 11. It appears that the separation of the EKWC and the generation of warm eddies are not much influenced

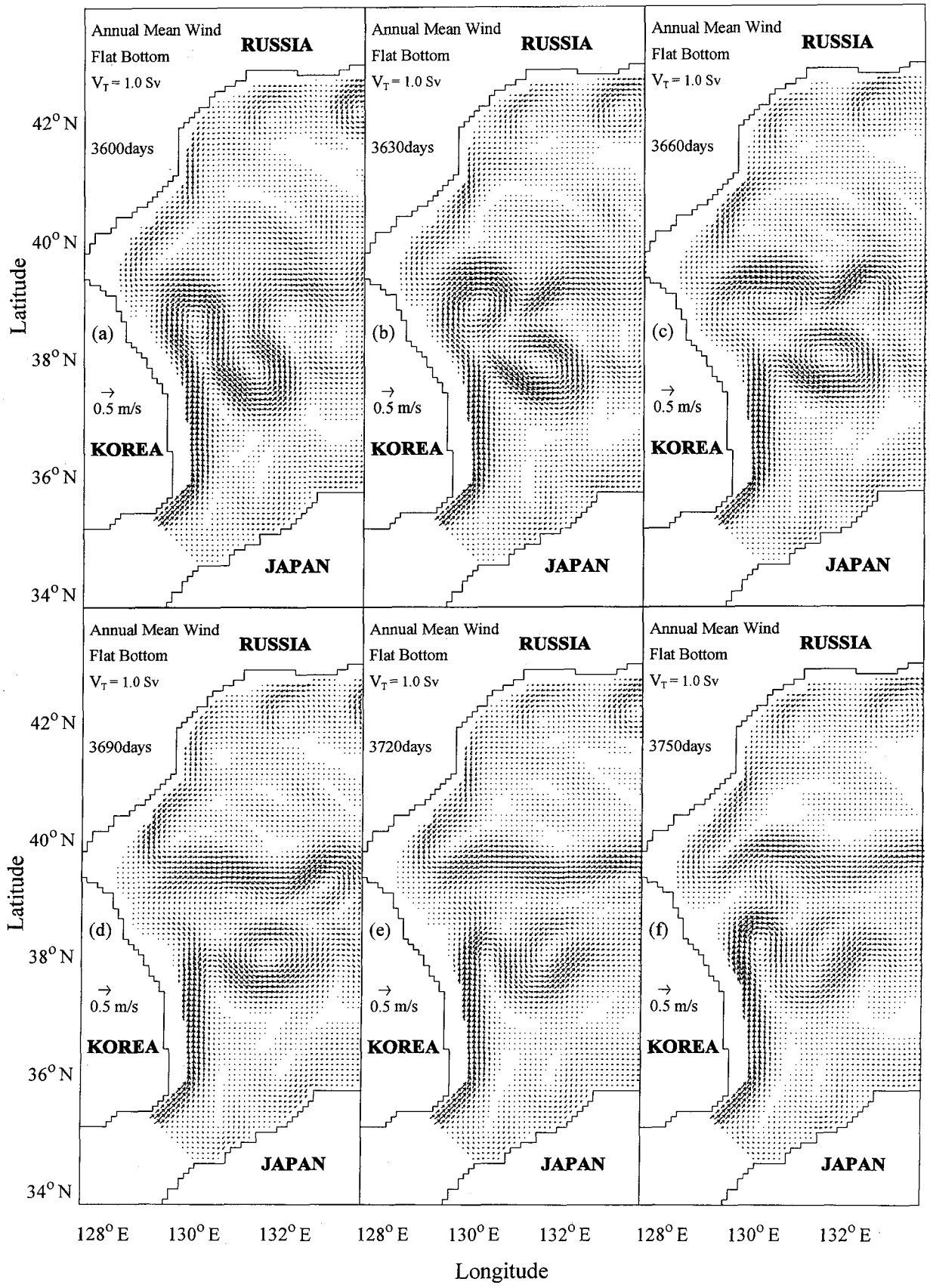

Fig. 9. A sequence of the upper layer flow from 3600 days to 3750 days when V_T=1.0Sv.

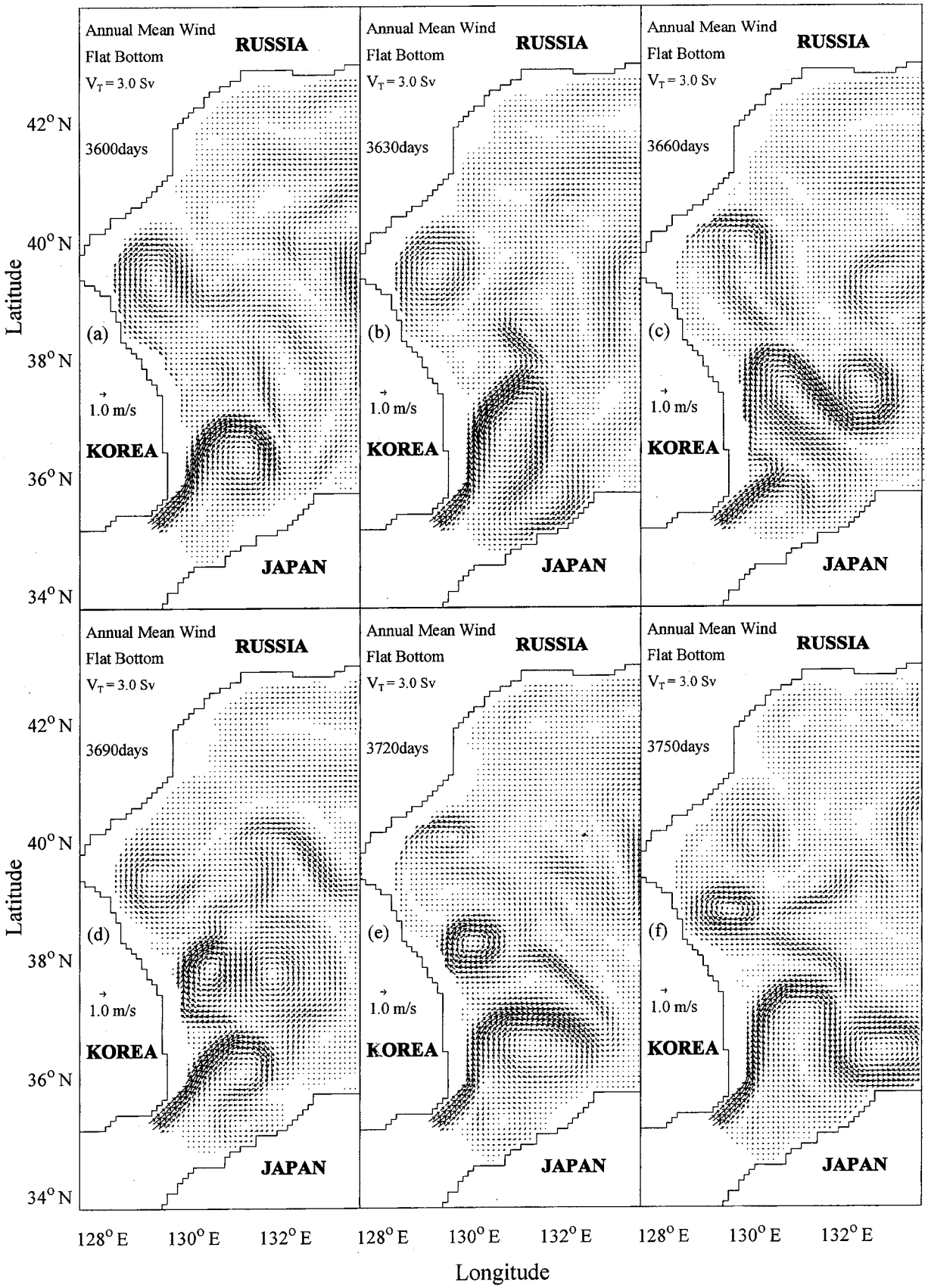

Fig. 10. A sequence of the upper layer flow from 3600 days to 3750 days when V_T=3.0Sv.

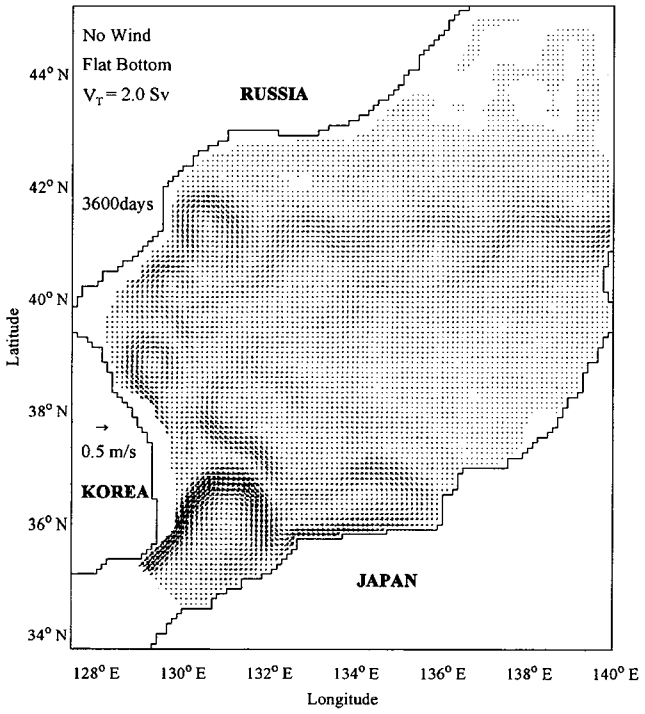

Fig. 11. The upper layer flow at 3600days for the no-wind case.

by the wind stress curl. Only difference from the preliminary case is that the warm eddy moved much northward up to 40°N. Accordingly, it can be concluded that the wind stress curl is not required to explain the EKWC separation and eddy generation.

Effect of seasonal forcing

From the preliminary model experiment, we found that the mesoscale eddies can be self-generated near the southwest of Ullung Island, with their formation and dissipation taking place in quite organized manner due to the instability and nonlinearity of the EKWC. However, it is not likely that the actual temporal change of the EKWC is such a regular process, not influenced by the time variation of the external forces. In fact, typical AVHRR images of the East Sea often show that the temporal and spatial patterns of the EKWC are indeed irregular. Therefore, in this section, we integrate the model with the seasonally varying wind curl (Fig. 12), and investigate how this seasonal wind changes the flow pattern, especially the separation of the EKWC and the generation of warm eddies.

Fig. 13 shows a sequence of the upper layer flow from 2520 to 2820 days driven by the seasonal wind stress curl. A striking feature different from the preliminary case is the wintertime intensification of the North Korea Cold Current (NKCC hereafter) during Jan/Mar with a maximum upper layer velocity of about 0.3 m/s. The flow pattern and the intensity of the simulated NKCC is compatible with the recent ADCP data presented by Isobe and Isoda (1997), implying that the NKCC is driven mostly by a positive wind stress curl in winter season (Na *et al.*, 1992). This aspect of the model result is, however, beyond the scope of this study, and it will not be discussed further. Apart from the seasonal intensification of the NKCC, it is clear that the separation latitude is highly irregular in time. It is note that the northward extent of the EKWC is influenced by the wintertime intensification of the NKCC. More specifically, during the winter season, the NKCC is developed by the cyclonic wind curl which in turn prevents the main branch of the EKWC or the separated warm eddy to move further northward. During other seasons, on the other hand, the NKCC is not well developed, therefore the EKWC and the warm eddies may freely extend much northward. This aspect of the model result is similar to the hypotheses proposed by Seung (1992b) and the numerical model result presented by Kim and Yoon (1996).

To further investigate the seasonal and inter-annual variation of the EKWC, we integrate the model up to 3960 days. Fig. 14 shows a sequence of the upper layer flow from 3600 to 3900days. Interestingly, comparing these with Fig. 13, it appears that there is no clear seasonal repetition in the spatial structure of the EKWC. For instance, the flow pattern in 3600 days (Jan/1) shows a separation of the EKWC at the sharp corner, but during the same month in Fig. 13 (2520 days), it shows a well developed EKWC with a separated offshore branch at aboutrm 39°N. This large interannual difference suggests that the separation of the EKWC and subsequent eddy generation may not be entirely driven by the changes of the external forces, but also to a considerable extent self-excited. The time-distance plot of the upper layer streamfunction along the line A (Fig. 15) also shows that the self-excited variability is significant in the model experiment.

SUMMARY AND DISCUSSION

The objective of this study was to simulate the

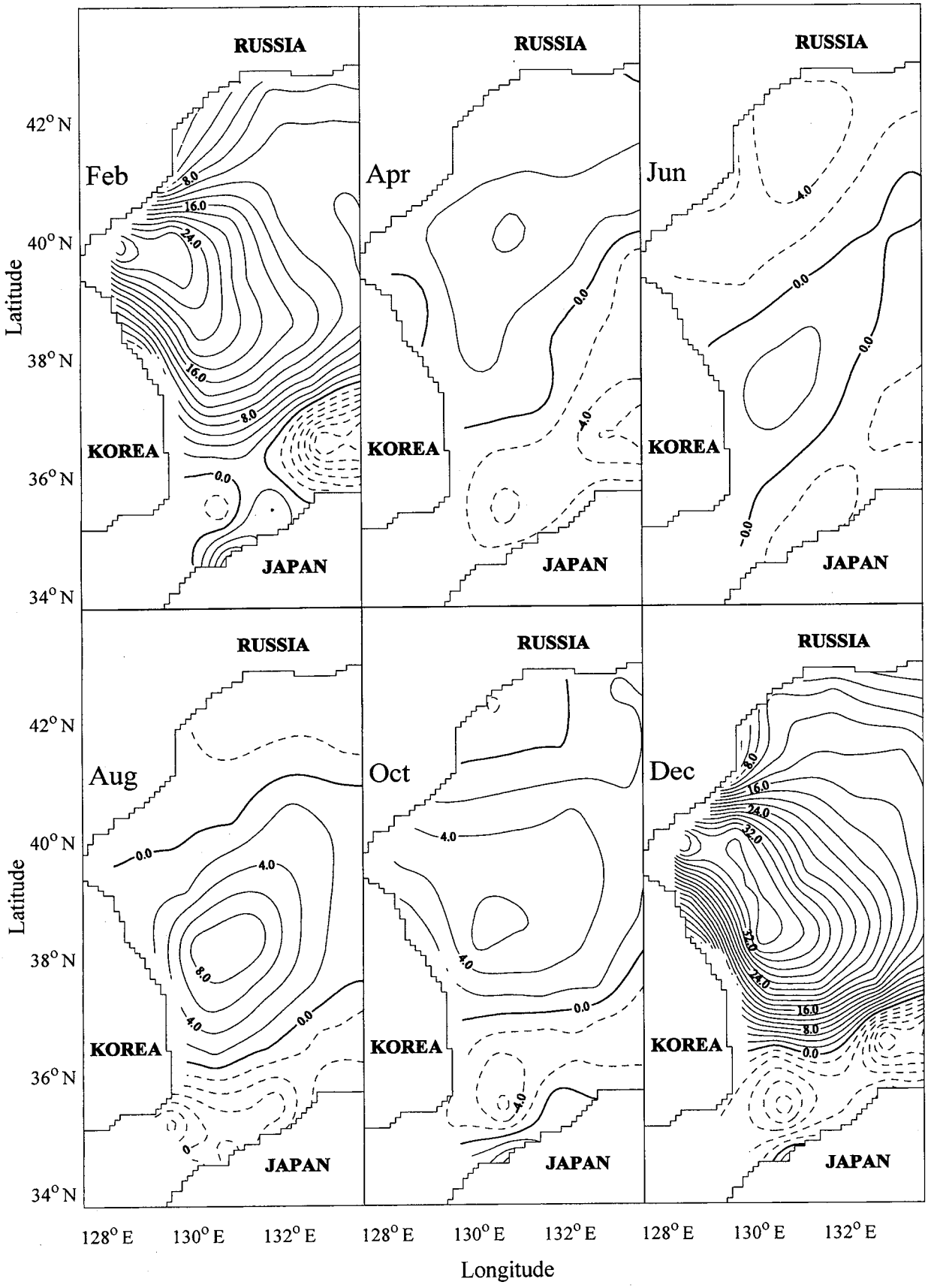

Fig. 12. Monthly averaged wind stress curl (Na *et al.*, 1992). The unit is 10^{-8}N/m^2.

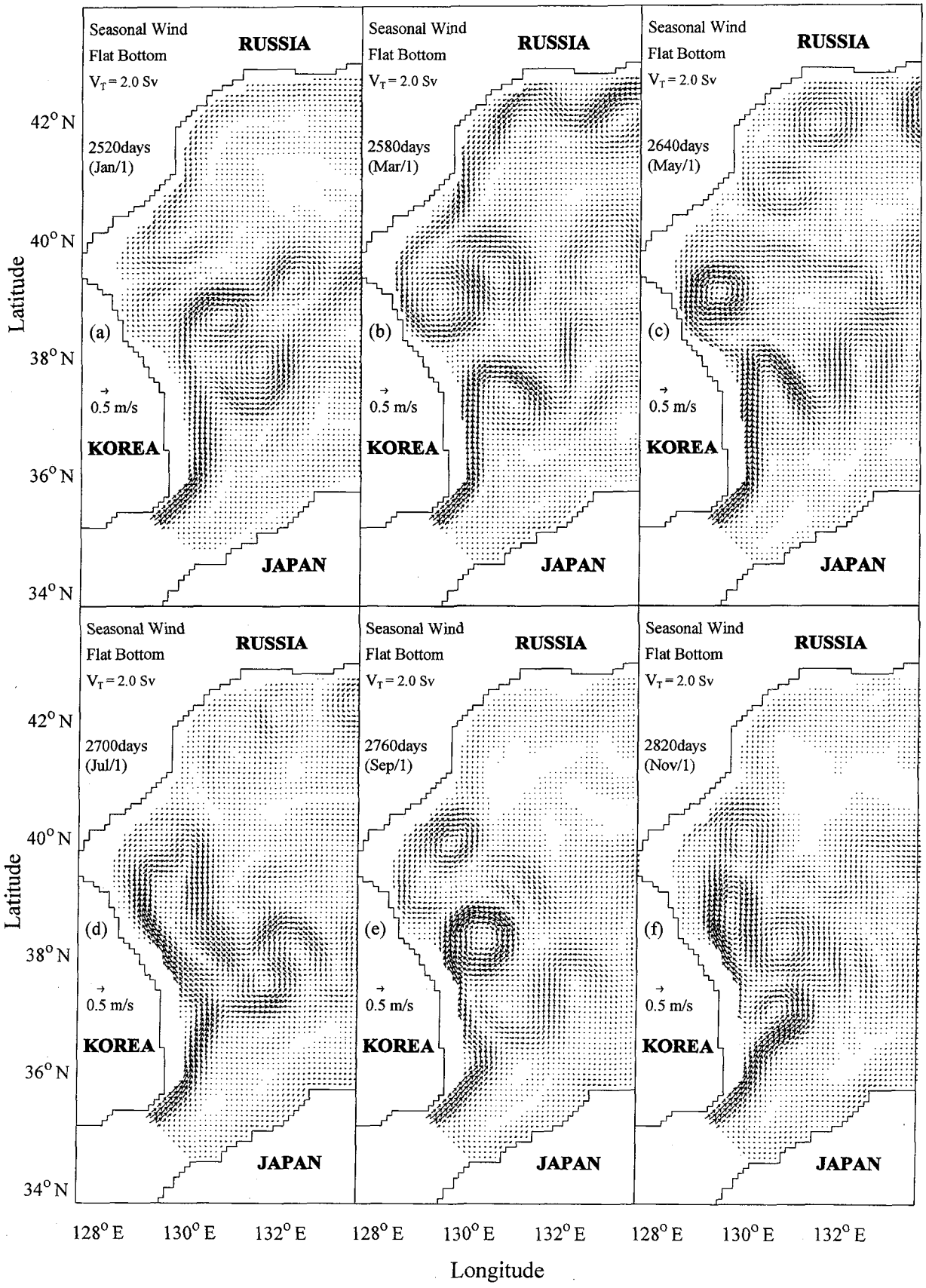

Fig. 13. A sequence of the upper layer flow from 2520 days to 2820 days for the seasonal wind case.

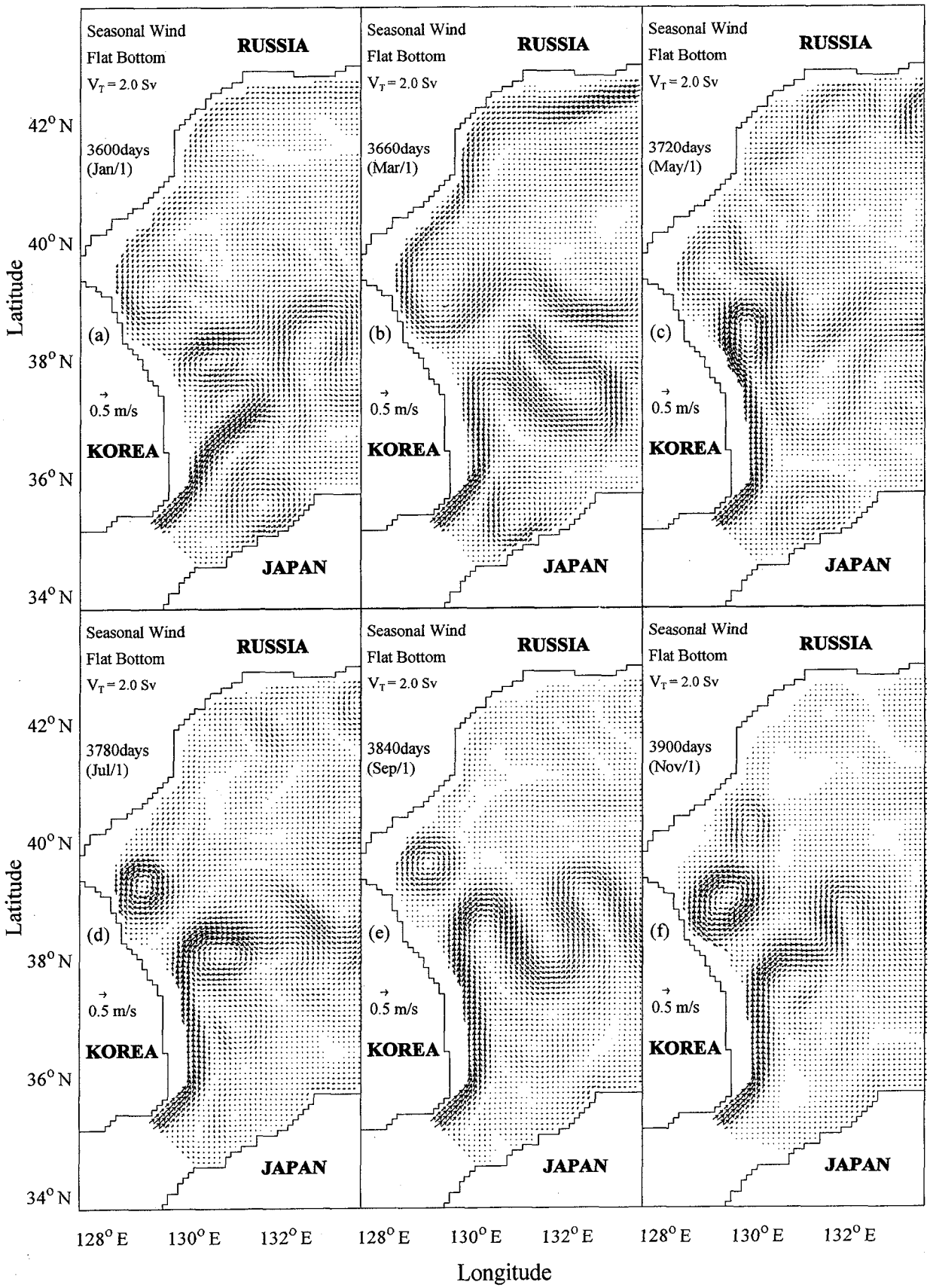

Fig. 14. A sequence of the upper layer flow from 3600 days to 3900 days for the seasonal wind case.

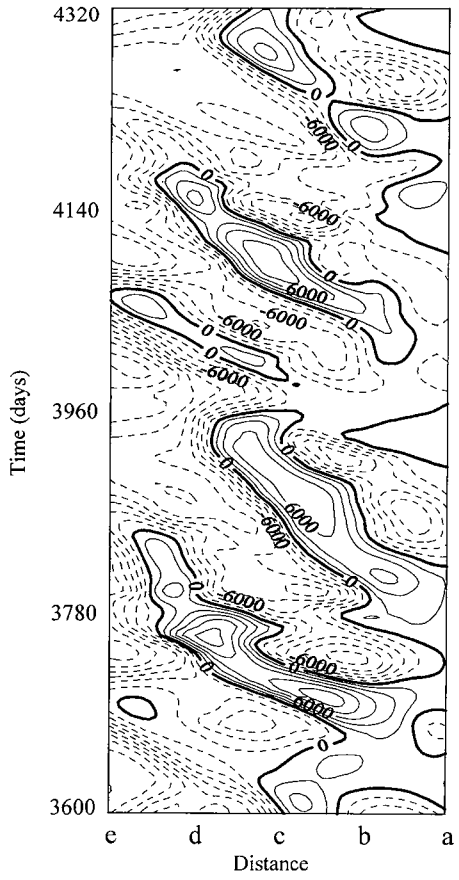

Fig. 15. A time-distance plot of the upper layer stream function along the line A for the seasonal wind case.

temporal variation of the EKWC, especially its separation from the Korean coast and subsequent generation of warm eddy, and to further understand its physics, using a two-layer quasi-geostrophic numerical model. The idealized flat bottom basin of the East Sea was forced by the annual mean wind curl, and the inflow-outflow via Korea and Tsugaru Straits.

The model results showed that the EKWC separates from the coast due to two different mechanisms. The first one is denoted as "externally driven separation" in which the separation is triggered when the southward flowing recirculation leg approaches the Korean coast. The second one is "internally driven separation" which is driven by wall boundary layer dynamics only. These two processes are not separable, and usually coexist. Similarly to the idea previously presented by Dengg (1993), it was hypothesized that the internally driven separation arises as the result of relative vorticity production at the wall, its subsequent advection via the EKWC, and its accumulation up to a critical level characterized by the separation of the boundary flow from the coast. It was suggested that the sharp southeastern corner of the Korean peninsula provides a favorable condition for the accumulation of relative vorticity. The model results also showed that a warm eddy is usually formed as the EKWC separates from the coast. The warm eddy is roughly 120 km in diameter, its typical layer-averaged velocity is about 0.3 m/s and its lifespan is less than one year, which are compatible with observations.

The effect of TC strength was investigated by comparing the two cases in which the volume transports at the input boundary (V_T) were fixed at 1.0Sv and 3.0Sv. When the transport is 1.0Sv, compared with the reference case, the separation latitude moves much northward at about 39°N, the flow is quite organized, and only one eddy is generated in one year period. On the other hand, when the transport is increased up to 3.0Sv, the separation takes place strictly at the convex corner, the northern limit of the EKWC excursion moves from 35°N to 38°N, the flow is less organized hardly repeating same spatial patterns in time, and approximately three eddies are generated in one year period. Therefore, it was concluded that, for the low Reynolds number flow, "externally driven separation" dominates, while "internally driven separation" plays a significant role for the high Reynolds number flow. The spatial profile, or preferably the potential vorticity, of the TC is assumed here to be determined by the volume transport (see Fig. 3). Therefore, the separation point and the strength of recirculation may be influenced by the different potential vorticity values of the TC fixed at the input boundary; however, this issue is not investigated further for simplicity.

The effect of seasonal wind curl was also investigated. It was shown that the northward intrusion of the EKWC or the warm eddy is restricted by the NKCC which is intensified in winter season, similar to the hypotheses proposed by Seung (1992b). Interestingly, however, the model results show no clear seasonal repetition in the spatial structure of the EKWC. This suggests that the separation of the EKWC and subsequent eddy generation may not be entirely driven by the changes of the external forces, but also to a certain degree self-excited.

By no means, the model experiment carried out in this study reflects the actual flow condition in the

East Sea, since there are many restrictions and assumptions in the model configuration. For instance, the potential effects of seasonally varying TC and wintertime convection were all neglected in the model study. But, the weakest aspect of the current model study lies on the exclusion of the bottom topography, since the EKWC have been long presumed to be influenced by the local topography, i.e., the Ullung basin (Cho *et al.*, 1990; Kim *et al.*, 1991). Because of these shortages in the current model, it is premature to fully apply the result of the model on the reality. Therefore, an extreme caution must be taken in interpreting the model result. Despite the lack of complexity in the model configuration, the model well reproduced certain features of the EKWC variability including the flow separation from the Korean coast and subsequent generation of warm eddy. More importantly, this model study showed the importance of the nonlinear boundary layer physics in the EKWC variability which has been usually disregarded in its interpretation. Additionally, it was emphasized that the variability of the EKWC can be self-excited, not being influenced by any sources of perturbation in the forcing field, contrary to the conclusion drawn by Lim and Kim (1995) who suggested that the primary source of the EKWC variability is the seasonal perturbation by the TC, although no observational evidence is currently available to clarify this point.

It is likely that the source of the self-excited variability is the barotropic instability by which the unstable eddies derive their energy from the horizontal shear of the EKWC (Pedlosky, 1979). However, more extensive study on the energy budget is required to estimate the relative importance of other instability mechanisms especially that of the baroclinic instability since the vertical shear may be important in the EKWC (Seung, 1992a). Other than this, further investigation of the bottom topography and thermohaline effect on the EKWC variability, especially the potential influence of the wintertime advection of cold subsurface water from the northern East Sea, with a higher vertical resolution model, may be a good extension of the current study.

Reviewers criticized that the grid resolution (10 km) is not fine enough to fully portray the viscous boundary layer (17 km), and insisted additional model runs with different values of eddy viscosity to justify the model result in the light of the AVHRR imageries shown in Fig. 7. While the coarse grid resolution may have distorted the viscous boundary layer solution to a measurable degree, since the model solutions are turbulent in nature it is likely that the time-averaged western boundary layer profile is determined by the Reynold stress flux $\partial(\overline{u'v'})/\partial x$, and that the eddy diffusion plays only a minor role.

ACKNOWLEDGMENTS

The arthur would like to thank Drs. Young-Ho Seung, Jose Pelegri, Soo-Yong Nam and two reviewers for valuable comments on the manuscript.

REFERENCES

An, H.S. and J.Y. Chung, 1982. The fluctuations of the thermal front in the southwestern area off Korea. *J. Oceanogr. Soc. Korea*, **17**: 33–40.

An, H.S., K. Shim and Shin H.R., 1994. On the warm eddies in the southwestern part of East Sea. *J. Oceanogr. Soc. Korea*, **29**: 152–163.

Arakawa, A., 1966. Computational design for long term numerical integration of the equations of fluid motion: two-dimensional incompressible flow. Part I. *J. Comput. Phys.* **1**: 119–143.

Cessi, P., G.R. Ierley and W. Young, 1987. A model of the inertial recirculation driven by potential vorticity anomalies. *J. Phys. Oceanogr.*, **17**: 1640–1652.

Charney, J.G., 1947. The dynamics of long waves in a baroclinic westerly current. *J. Meteor.*, **4**: 135–163.

Csanady, G.T., 1989. Energy dissipation and upwelling in a western boundary current. *J. Phys. Oceanogr.*, **19**: 462–473.

Cummins, P.F. and L.A. Mysak, 1988. A quasi-geostrophic model of the northeast pacific. Part I: a preliminary numerical experiment. *J. Phys. Oceanogr.*, **18**: 1261–1286.

Dengg, J., 1993. The problem of Gulf Stream separation: A barotropic approach. *J. Phys. Oceanogr.*, **23**: 2182–2200.

Eady, E.T., 1949. Long waves and cyclone waves. *Tellus*, **1**: 33–52.

Egawa, T., Y. Nagata and S. Sato, 1993. Seasonal variation of the current in the Tsushima Strait deduced from ADCP data of ship-of-opportunity. *J. Oceanogr.*, **49**: 39–50.

Foreman, M.G.G. and A.F. Bennett, 1988. On no-slip boundary conditions for the incompressible Navier-Stokes equations. *Dyn. Atms. Oceans*, **12**: 47–70.

Gong, Y. and S.Y. Son, 1982. A study of oceanic thermal fronts in the south-western Japan Sea. *Bull. Fish. Res. Develop. Agency*, **4**: 69–91.

Hidaka, K. and T. Suzuki, 1950. Secular variation of the Tsushima Current. *J. Oceanogr. Soc. Japan*, **16**: 28–31 (in Japanese).

Holland, W.R., 1978. The role of mesoscale eddies in the general circulation of the ocean-numerical experiments using a wind-driven quasi-geostrophic model. *J. Phys. Oceanogr.*, **8**: 363–392.

Holland, W.R., 1986. Quasigeostrophic modelling of eddy-resolved ocean circulation. In: Advanced physical oceanographic numerical modelling, edited by J.J. O'Brien, Reidel, Dordrecht, 608pp.

Hong, C.H. and K.D. Cho, 1983. The northern boundary of the Tsushima Current and its fluctuations. *J. Oceanogr. Soc. Korea*, **18**: 1–9.

Ierley, G.R. and W.R. Young, 1991. Viscous instabilities in the western boundary layer. *J. Phys. Oceanogr.* **21**: 1323–1332.

Isobe, A., 1994. Seasonal variability of the barotropic motion in the Tsushima-Korea Strait. *J. Oceanogr.* **50**: 223–238.

Isobe, A., S. Tawara, A. Kaneko and M. Kawano, 1994. Seasonal variability in the Tsushima Warm Current, Tsushima-Korea Strait. *Cont. Shelf Res.*, **14**: 23–35.

Isobe, A. and Y. Isoda, 1997. Circulation in the Japan Basin, the northern part of the Japan Sea. *J. Oceanogr.*, **53**: 373–381.

Isoda, Y. and S. Saitoh, 1993. The northward intruding eddy along the east coast of Korea. *J. Oceanogr.*, **49**: 443–458.

Kaneko, A., S.K. Byun, S.D. Chang and M. Takahashi, 1991. An Observation of Sectional Velocity Structures and Transport of the Tsushima Current across the Korea Strait. In: Oceanography of Asian Marginal Seas, edited by K. Takano, Elsevier Sci. Pub., Amsterdam, 179–195.

Kawabe, M., 1982. Branching of the Tsushima Current in the Japan Sea. Part II: Numerical experiment. *J. Oceanogr. Soc. Japan*, **38**: 183–192.

Kawano, M., 1993. Monthly changes of velocity and volume transport of the Tsushima Warm Current in the Tsushima Strait. *Bull. Japan Soc. Fish. Oceanogr.*, **57**: 219–230 (in Japanese).

Kim, C.H., 1996. A numerical experiment study on the circulation of the Japan Sea (East Sea). Ph.D. thesis, Kyushu Univ., Fukuoka, 151pp.

Kim, C.H. and J.H. Yoon, 1996. Modelling of the wind driven circulation in the Japan Sea using a reduced gravity model. *J. Oceanogr.*, **52**: 359–373.

Kim, K and R. Legeckis, 1986. Branching of the Tsushima Current in 1981–83. *Prog. Oceanogr.*, **17**: 265–276.

Kim, K., K.R. Kim, J.Y. Chung, H.S. Yoo and S.G. Park, 1991. Characteristics of physical properties in the Ullung Basin. *J. Oceanogr. Soc. Korea*, **26**: 83–100.

Kim, Y.E., 1991. A numerical study on the circulation of the East Sea (Japan Sea). Ph.D. thesis, Seoul National University, Seoul, 211pp.

Lie, H.J. and Y.H. Seung, 1994. A review on status and development of physical oceanography research in Korea. *J. Oceanogr. Soc. Korea*, **29**: 64–81.

Lim, K.S. and K. Kim, 1995. A numerical study on the interaction of Ullung warm eddy with topography and lateral boundary. *J. Oceanogr. Soc. Korea*, **30**: 565–583.

McWilliams, J.C. 1977. A note on a consistent quasigeostrophic model in a multiply connected domain. *Dyn. Atmos. Oceans*, **1**: 427–441.

Moriyasu, S., 1972. The Tsushima Current. In: The Kuroshio - its physical Aspects, edited by H. Stommel and K. Yoshida, Tokyo University Press, Tokyo, 353–369.

Munk, W.H., 1950. On the wind-driven ocean circulation. *J. Meteor.*, **7**: 79–93.

Na, J.Y., J.W. Seo and S.K. Han, 1992. Monthly-mean surface winds over the adjacent seas of the Korea peninsula. *J. Oceanogr. Soc. Korea*, **27**: 1–10.

Pedlosky, J., 1979. Geophysical Fluid Dynamics. Springer-Verlag, New York, 624pp.

Prandtl, L., 1935. The Mechanics of Viscous Fluids, Aerodynamic theory, edited by W.F. Durand, Springer, Berlin, 34–208.

Press, W.H., S.A. Teukolsky, W.T. Vetterling and B.P. Flannery, 1992. Numerical Recipes in FORTRAN - the Art of Scientific computing (2nd ed.), Cambridge University Press, New York, 963pp.

Richtmyer, R.D., 1967. Difference Methods for Initial-value problems (2nd ed.), Interscience, 405pp.

Roache, P.J., 1976. Computational Fluid Dynamics, Hermosa, New Maxico, 446pp.

Seung, Y.H. and K. Kim, 1989. On the possible role of local thermal forcing on the Japan Sea circulation. *J. Oceanogr. Soc. Korea*, **24**: 29–38.

Seung, Y.H., 1992a. Water masses and circulations around Korean peninsula. *J. Oceanogr. Soc. Korea*, **27**: 324–331.

Seung, Y.H., 1992b. A simple model for separation of East Korea Warm Current and Formation of North Korea Cold Current. *J. Oceanogr. Soc. Korea*, **27**: 189–196.

Seung, Y.H. and K. Kim, 1993. A numerical modeling of the East Sea circulation. *J. Oceanogr. Soc. Korea*, **28**: 292–304.

Seung, Y.H. and K.J. Kim, 1995. A multilayer model for dynamics of upper and intermediate layer circulation of the East Sea. *J. Oceanogr. Soc. Korea*, **30**: 227–236.

Seung, Y.H. and K.J. Kim, 1997. Estimation of the residence time for renewal of the East Sea intermediate water using MICOM. *J. Oceanogr. Soc. Korea*, **32**: 17–27.

Seung Y.H. and S.Y. Nam, 1992. A two-layer model for the effect of cold water formation on the East Korea Warm Current. *Bull. Korean Fish. Soc.*, **25**: 65–72.

Shin, H.R., S.K. Byun, C. Kim and S. Hwang and C.W. Shin, 1995. The characteristics of structure of warm eddy observed to the northwest of Ullungdo in 1992. *J. Oceanogr. Soc. Korea*, **30**: 39–56.

Suda, K. and K. Hidaka, 1932. The results of the oceanographical observations on board RMS Syunpu Maru in the southern part of the Japan Sea in summer, 1929. *J. Oceanogr.*, **3**: 291–375.

Toba, Y., K. Tomizawa, Y. Kurasawa and K. Hanawa, 1982. Seasonal and year-to-year variability of the Tsushima-Tsugaru Warm Current system with its possible cause. *La Mer*, **20**: 41–51.

Uda, M., 1934. The results of simultaneous oceanographical investigations in the Japan Sea and its adjacent waters in May and June, 1932. *J. Imp. Fish. Exp. Sta.*, **5**: 57–190 (in Japanese).

Verron, J. and E. Blayo, 1996. The no-slip condition and the separation of western boundary currents. *J. Phys. Oceanogr.*, **26**: 1938–1951.

Yi, S.W., 1966. Seasonal and secular variations of the water volume transport across the Korea Strait. *J. Oceanogr. Soc. Korea*, **1**: 1–6.

Yoon, J.H., 1982. Numerical experiments on the circulation in the Japan Sea, Part III: Formation of the nearshore branch of the Tsushima Current. *J. Oceanogr. Soc. Japan*, **38**: 119–124.

Manuscript received July 13, 1998
Revision accepted December 17, 1998

APPENDIX A. METHOD OF SOLUTION

Using Eqns. (2)~(6), Eqn. (1) can be rewritten as

$$\frac{\partial}{\partial t}\left[\nabla^2\psi_k+\frac{f_o^2}{g'_{k-\frac{1}{2}}H_k}\psi_{k-1}-\left(\frac{f_o^2}{g'_{k-\frac{1}{2}}H_k}+\frac{f_o^2}{g'_{k+\frac{1}{2}}H_k}\right)\psi_k+\frac{f_o^2}{g'_{k+\frac{1}{2}}H_k}\psi_{k+1}\right]=r_k \quad \text{(A1)}$$

where

$$\begin{aligned} r_k =& J(\nabla^2\psi_k, \psi_k)-\beta\frac{\partial\psi_k}{\partial x}+\frac{f_o^2}{g'_{k-\frac{1}{2}}H_k} \\ & J(\psi_{k-1}-\psi_k, \psi_{k-\frac{1}{2}})-\frac{f_o^2}{g'_{k+\frac{1}{2}}H_k} \\ & J(\psi_k-\psi_{k+1}, \psi_{k+\frac{1}{2}})+A_h\nabla^4\psi_k-\delta_{N,k}\varepsilon\nabla^2\psi_k \\ & +\delta_{1,k}\frac{\mathrm{curl}_z\,\tau}{\rho_1 H_1}-\delta_{N,k}\frac{f_o}{H_k}J(\psi_k, h_B), \end{aligned} \quad \text{(A2)}$$

In matrix form, Eqn. A1 becomes

$$\frac{\partial}{\partial t}(\nabla^2\boldsymbol{\Psi}-\mathbf{M}\boldsymbol{\Psi})=\mathbf{R}, \quad \text{(A3)}$$

Because the layer equations are coupled with each other, an efficient method of solving them is to transform the equations to modal form, which in turn decouples the equations (Cummins and Mysak, 1988). The transformation is performed by diagonalizing matrix **M**.

First, we must find eigenvalues λ:

$$\begin{bmatrix} \alpha_{1,1} & \alpha_{1,2} & \cdots & \alpha_{1,N} \\ \alpha_{2,1} & \alpha_{2,2} & \cdots & \alpha_{2,N} \\ \cdot & \cdot & \cdots & \cdot \\ \cdot & \cdot & \cdots & \cdot \\ \alpha_{N,1} & \alpha_{N,2} & \cdots & \alpha_{N,N} \end{bmatrix} \begin{bmatrix} x_1 \\ x_2 \\ \cdot \\ \cdot \\ x_N \end{bmatrix} = \begin{bmatrix} \lambda & 0 & \cdots & 0 \\ 0 & \lambda & \cdots & 0 \\ \cdot & \cdot & \cdots & \cdot \\ \cdot & \cdot & \cdots & \lambda \\ 0 & 0 & \cdots & \lambda \end{bmatrix} \begin{bmatrix} x_1 \\ x_2 \\ \cdot \\ \cdot \\ x_N \end{bmatrix}, \quad \text{(A4)}$$

The elements of the matrix **M** are

$$\begin{aligned} \alpha_{k,k-1} &= -\frac{f_o^2}{g'_{k-\frac{1}{2}}H_k}, \\ \alpha_{k,k} &= \frac{f_o^2}{g'_{k-\frac{1}{2}}H_k}+\frac{f_o^2}{g'_{k+\frac{1}{2}}H_k}, \\ \alpha_{k,k+1} &= -\frac{f_o^2}{g'_{k+\frac{1}{2}}H_k}, \end{aligned} \quad \text{(A5)}$$

Since the matrix **M** is a tridiagonal matrix, a special form of Hessenberg Matrix, the QR algorithm maybe applied to evaluate eigenvalues (Press *et al.*, 1992). Once the eigenvalues are determined, the Gauss-Jordan elimination is used to calculate corresponding eigenvectors. If **P** represent a matrix whose columns are the eigenvectors and Λ a diagonal matrix of eigenvalues, we get

$$\mathbf{MP}=\mathbf{P}\Lambda, \quad \text{(A6)}$$

or equivalently

$$\mathbf{M}=\mathbf{P}\Lambda\mathbf{P}^{-1}, \quad \text{(A7)}$$

substituting Eqn. A7 into A3, we get

$$\frac{\partial}{\partial t}(\nabla^2\boldsymbol{\Psi}-\mathbf{P}\Lambda\mathbf{P}^{-1}\boldsymbol{\Psi})=\mathbf{R}, \quad \text{(A8)}$$

$$\frac{\partial}{\partial t}(\nabla^2\mathbf{P}^{-1}\boldsymbol{\Psi}-\Lambda\mathbf{P}^{-1}\boldsymbol{\Psi})=\mathbf{P}^{-1}\mathbf{R}, \quad \text{(A9)}$$

$$\frac{\partial}{\partial t}(\nabla^2\boldsymbol{\Phi}-\Lambda\boldsymbol{\Phi})=\mathbf{S}, \quad \text{(A10)}$$

where $\boldsymbol{\Psi}=\mathbf{P}^{-1}\boldsymbol{\Phi}$. Eqn. A10 gives the rate of change of each mode, which can be used to march step forward in time.

At wall boundaries, following relationship applies,

$$\psi_k(\mathrm{wall}_2)-\psi_k(\mathrm{wall}_1)=V_k \quad \text{(A11)}$$

where wall_1 and wall_2 represent sidewalls of Korean and Japanese continents, respectively, and V_k is the volume transport through inflow-outflow boundaries.

If $a^1_{i,j}$ and $a^2_{i,j}$ are elements of matrix **P** and $\mathbf{P}^{-1}$ respectively, it is convenient to set solution form as

$$\begin{bmatrix} \psi_1 \\ \psi_2 \\ \cdot \\ \cdot \\ \psi_N \end{bmatrix} = \begin{bmatrix} a^1_{1,1} & a^1_{1,2} & \cdots & a^1_{1,N} \\ a^1_{2,1} & a^1_{2,2} & \cdots & a^1_{2,N} \\ \cdot & \cdot & \cdots & \cdot \\ \cdot & \cdot & \cdots & \cdot \\ a^1_{N,1} & a^1_{N,2} & \cdots & a^1_{N,N} \end{bmatrix} \begin{bmatrix} \phi_{1a}+C_1\phi_{1c} \\ \phi_{2a}+C_2\phi_{2c} \\ \cdot \\ \cdot \\ \phi_{Na}+C_N\phi_{Nc} \end{bmatrix} + \begin{bmatrix} V_1\psi_{1b} \\ V_2\psi_{2b} \\ \cdot \\ \cdot \\ V_N\psi_{Nb} \end{bmatrix}, \quad \text{(A12)}$$

where ϕ_k is set as

$$\phi_k = \phi_{ka} + C_k \phi_{kc} + \sum_{j=1}^{N} a_{k,j}^2 V_j \psi_{jb}, \tag{A13}$$

and ϕ_{ka}', ϕ_{kc} must satisfy followings,

$$\nabla^2 \boldsymbol{\Phi}_a' - \boldsymbol{\Lambda} \boldsymbol{\Phi}_a' = \boldsymbol{S}\ , \tag{A14}$$

$$\nabla^2 \boldsymbol{\Phi}_c - \boldsymbol{\Lambda} \boldsymbol{\Phi}_c = 0\ , \tag{A15}$$

with boundary conditions of

$$\begin{aligned} &\phi_{ka}(\text{wall}) = 0, \\ &\phi_{kc}(\text{wall}) = 1, \\ &\phi_{ka}'(\text{wall}) = 0, \end{aligned} \tag{A16}$$

where the prime represents time differential. The function ϕ_{kb} must be determined according to initial conditions, and the boundary conditions of

$$\phi_{kb}(\text{wall}_1) = 0, \tag{A17}$$

$$\phi_{kb}(\text{wall}_2) = 1, \tag{A18}$$

Continuity of each layer requires that spatial integration of interface variation must vanishes. i.e.,

$$\iint_\Omega \frac{\partial}{\partial t}(\psi_k - \psi_{k+1}) dxdy = 0, \text{ for k=1, 2, } \cdots\text{, N-1 .} \tag{A19}$$

Since the vertical velocity is associated strictly with baroclinic modes, equivalent to Eqn. A19 is

$$\iint_\Omega \frac{\partial \phi_k}{\partial t} dxdy = 0, \text{ for k=2, } \cdots\text{, N,} \tag{A20}$$

or using A13, we get

$$\begin{aligned} &\iint_\Omega [\phi_{ka} + C_k \phi_{kc} + \sum_{j=1}^{N} a_{k,j}^2 V_j \psi_{jb}] dxdy \\ &\quad = \iint_\Omega \phi_{ko}\, dxdy, \quad \text{for k=2, } \cdots\text{, N,} \end{aligned} \tag{A21}$$

where ϕ_{ko} represent initial condition for each mode variables. Without losing a generality we set C_1 (barotropic mode) equal to zero. Then we get

$$C_k = \frac{\iint_\Omega \left[\phi_{ko} - \phi_{ka} - \sum_{j=1}^{N} a_{k,j}^2 V_j \psi_{jb} \right] dxdy}{\iint_\Omega \phi_{kc}}, \quad \text{for k=2, } \cdots\text{, N.} \tag{A22}$$